

The tuned mass-damper-inerter for harmonic vibrations suppression, attached mass reduction, and energy harvesting

Laurentiu Marian^{1a} and Agathoklis Giaralis^{*2}

¹AKT-II Ltd, 100 St John Street, EC1M 4EH, London, UK

²Department of Civil Engineering, City, University of London, Northampton Square, EC1V 0HB, UK

(Received October 30, 2016, Revised May 2, 2017, Accepted May 12, 2017)

Abstract. In this paper the tuned mass-damper-inerter (TMDI) is considered for passive vibration control and energy harvesting in harmonically excited structures. The TMDI couples the classical tuned mass-damper (TMD) with a grounded inerter: a two-terminal linear device resisting the relative acceleration of its terminals by a constant of proportionality termed inertance. In this manner, the TMD is endowed with additional inertia, beyond the one offered by the attached mass, without any substantial increase to the overall weight. Closed-form analytical expressions for optimal TMDI parameters, stiffness and damping, given attached mass and inertance are derived by application of Den Hartog's tuning approach to suppress the response amplitude of force and base-acceleration excited single-degree-of-freedom structures. It is analytically shown that the TMDI is more effective from a same mass/weight TMD to suppress vibrations close to the natural frequency of the uncontrolled structure, while it is more robust to detuning effects. Moreover, it is shown that the mass amplification effect of the inerter achieves significant weight reduction for a target/predefined level of vibration suppression in a performance-based oriented design approach compared to the classical TMD. Lastly, the potential of using the TMDI for energy harvesting is explored by substituting the dissipative damper with an electromagnetic motor and assuming that the inertance can vary through the use of a flywheel-based inerter device. It is analytically shown that by reducing the inertance, treated as a mass/inertia-related design parameter not considered in conventional TMD-based energy harvesters, the available power for electric generation increases for fixed attached mass/weight, electromechanical damping, and stiffness properties.

Keywords: tuned mass damper; inerter; passive vibration control; energy harvesting; weight reduction; electromagnetic motor; optimal design

1. Introduction

The concept of the dynamic vibration absorber (DVA) is historically one of the first strategies for passive vibration control of dynamically excited mechanical and civil engineering structures and structural components (Frahm 1911). It relies on attaching a free-to-vibrate mass to the structural system whose motion is to be suppressed (primary structure), such that significant kinetic energy is transferred from the primary structure to the attached mass. Considering a linear spring in parallel with a dashpot (e.g., a linear viscous damper) to attach the vibrating mass to the primary structure, the so-called tuned mass-damper (TMD) is, arguably, the most widely studied passive DVA in the literature (e.g., Ormondroyd and Den Hartog 1928, Brock 1946, Den Hartog 1956, Warburton 1982, Rana and Soong 1998, Asami *et al.* 2002, Krenk 2005, Ghosh and Basu 2007, Bakre and Jangid 2007, Leung and Zhang 2009, Tributch and Adam 2012, Bortoluzzi *et al.* 2015, Salvi and Rizzi 2016) and the most commonly used in practical

applications. The widespread use of the classical linear TMD is mainly due to the existence of simple and well-established design approaches seeking to determine optimal TMD stiffness and damping properties that minimize the response of a given dynamically excited primary structure for an *a priori* fixed attached mass. Focusing on periodic narrow-band excitations, Den Hartog (1956) established a semi-empirical TMD design approach by relying on the observation that all frequency response functions (FRFs) of a TMD-equipped undamped single degree-of-freedom (SDOF) primary structure pass through the same two points. Based on this "fixed point" theory, Den Hartog (1956) and Brock (1946) reached simple closed-form expressions for the TMD stiffness and damping properties, widely used in practical TMD design, to suppress the peak displacement of sinusoidal force-excited undamped SDOF primary structures (see also Krenk 2005). Further, Warburton (1982) followed the above design approach to derive TMD design formulae minimizing different response quantities of interest for harmonic force and base-excited undamped SDOF primary structures. More recently, Ghosh and Basu (2007) demonstrated that the fixed point theory leads to near-optimal TMD vibration suppression performance for the case of lightly damped SDOF primary structures with critical damping ratio up to 3%, applicable to a wide range of structures and structural components. Notably, the above TMD design formulae can be further

*Corresponding author, Senior Lecturer
E-mail: Agathoklis.Giaralis.1@city.ac.uk

^aPh.D.
E-mail: Laurentiu.Marian.1@akt-uk.com

applied to suppress the vibratory motion corresponding to a single (e.g., the dominant) structural mode shape in the case of lightly damped multi degree-of-freedom (MDOF) primary structures (e.g., Rana and Soong 1998).

Further to vibration suppression, the potential of the TMD to harvest energy from large-amplitude low-frequency oscillating primary structures has been recently recognized (Rome *et al.* 2005) and explored by various researchers focusing primarily on large-scale (civil engineering) primary structures. In particular, TMDs can achieve simultaneous vibration suppression and energy generation by employing either electromagnetic (EM) devices (e.g., Tang and Zuo 2012, Shen *et al.* 2012, Zuo and Tang 2013, Gonzalez-Buelga *et al.* 2014, Shen *et al.* 2016), or piezo-electric materials (e.g., Adhikari and Ali 2013) to connect the TMD mass to the primary structure as opposed to using only dampers. In this manner, part of the kinetic energy of the primary structure is transformed into electric energy instead of being “lost” at the dampers in the form of heat. The thus generated energy may be stored to batteries for later use (Zuo and Tang 2013), or can be used to achieve energy-autonomous semi-active or even active TMD vibration control strategies (Tang and Zuo 2012, Gonzalez-Buelga *et al.* 2014), or to power wireless sensors for structural health monitoring (Shen *et al.* 2012, Makiyara *et al.* 2015).

Despite being widely used in practice, the classical (linear passive) TMD is known to suffer from the problem of “detuning” due to such reasons as nonlinear behaviour of the primary structure (e.g., Domizio *et al.* 2015), and/or uncertainty and variations to the dynamic properties of the primary structure over time (e.g., Wang and Lin 2015). Detuning affects significantly the TMD vibration suppression performance (and consequently its potential for energy harvesting), especially for the case of harmonic/narrow band excitations as its effectiveness depends heavily on ensuring resonance between the primary structure and the TMD. To this end, different strategies have been considered to enhance the robustness to detuning of the *passive* TMD for the purpose of controlling a single primary structure vibration mode. One such strategy is to use hysteretic/yielding components to attach the TMD mass to the primary structure (e.g., Ricciardeli and Vickery 1999) which widens the operational TMD frequency range around the target primary structure natural frequency. Nevertheless, optimal design of inelastic TMDs is considerably more challenging compared to the linear TMD. Alternatively, robustness to detuning effects can be achieved by use of multiple TMDs (MTMDs) linked in parallel (e.g., Xu and Igusa, 1992, Yamaguchi and Harnpornchai 1993) or in series (Zuo 2009). In the parallel configuration, each individual TMD is tuned to a different frequency such that the effective frequency band becomes wider. In the series configuration, a chain of two or more appropriately determined masses are attached to the primary structure and tuned to achieve “multiple resonance” at the cost of excessive attached mass displacements. Parallel MTMDs have been considered for wind-induced vibration suppression in piers of cable-stayed bridges (Casciati and Giuliano 2009) and for traffic-induced vibrations

suppression in (foot-)bridges (e.g., Lin *et al.* 2005), among other applications. Nevertheless, optimal MTMD design is appreciably more involved than single TMD design (see e.g., Jokic *et al.* 2011) due to the increased number of design variables, while heuristic/experiential assumptions need to be made for the mass distribution among the TMDs (see e.g., Bandivadekar and Jangid 2012, Yang *et al.* 2015).

To this end, it is argued that, perhaps, the simplest and most straightforward way to enhance the performance and robustness to detuning of the classical single TMD is to increase the attached mass for which “optimum” stiffness and damping parameters is sought in TMD design. Indeed, the larger the attached TMD mass considered, the more effective an optimally designed linear TMD becomes to suppress excessive primary structure vibrations and the less sensitive to detuning effects (see e.g., De Angelis *et al.* 2012 and references therein). Nevertheless, these benefits come at the cost of an increase total weight of the overall TMD-equipped structural system. To circumvent the latter trade-off, this paper considers coupling the classical linear TMD with an inerter device, introduced by Smith (2002), in a so-called “sky-hook” configuration as has been recently proposed by the authors (Marian and Giaralis 2014). In this manner, the resulting tuned mass-damper-inerter (TMDI) configuration exploits the mass amplification effect of the inerter (i.e., a linear two-terminal device of negligible mass/weight which resists the relative acceleration of its terminals) to increase the inertia of the attached mass, without increasing the overall weight of the controlled structure. In fact, the authors showed that for the same attached mass the TMDI performs better than the classical TMD, treated as a special case of the TMDI, in suppressing the displacement variance of stochastically based-excited SDOF and MDOF primary structures (Marian and Giaralis 2013, 2014). More recently, the potential of the TMDI for the seismic protection of primary structures modelled as SDOF systems has been explored by Pietrosanti *et al.* (2017) and by Masri and Caffrey (2017), while Giaralis and Petrini (2017) considered the use of TMDI for wind-induced vibration mitigation in a benchmark tall building accounting for vortex shedding effects.

Herein, closed-form formulae are derived for optimal TMDI design in harmonically excited undamped SDOF primary structures based on the fixed point theory. These formulae are then used to quantify the gains in terms of vibration suppression and of weight reduction for optimally designed TMDI vis-à-vis the classical TMD. Further, the incorporation of a linear electromagnetic motor shunted by a resistive load is considered to gauge the potential of the TMDI for energy harvesting. This is analytically assessed by assuming the availability of a flywheel-based inerter device with varying mass amplification property. The latter consideration introduces a new “degree of freedom” which allows to vary the apparent inertia of the energy harvester leveraging the trade-off between vibration suppression and energy harvesting at will, without any changes to the attached mass.

Overall, apart from the novel closed-form expressions for the TMDI design for harmonic excitations, this paper makes original contributions by analytically quantifying (1)

the vibration suppression performance enhancement of the TMDI compared to the classical TMD in harmonically force-excited and support-excited primary structures, (2) the weight reduction achieved by the TMDI compared to the classical TMD as a function of the inerter mass amplification property for a predefined vibration suppression performance, and (3) the increase of the available electric power to be generated from harmonically excited primary structures by employing a passive energy harvesting enabled TMDI with varying inertance.

The remainder of the paper is organized as follows. In Section 2 the ideal flywheel-based inerter is briefly presented and the governing equations of motion and associated frequency response functions of TMDI equipped SDOF primary structures are furnished. In Section 3, closed-form expressions for the design of the TMDI for harmonically excited primary structures are derived based on the fixed point theory and the benefits of the TMDI vis-à-vis the TMD in terms of vibration suppression and weight reduction are analytically quantified. Section 4 introduces an energy harvesting enabled TMDI and quantifies analytically its vibration suppression and power generation capabilities for harmonically excited primary structures, while Section 5 quantifies the increase to the available energy for harvesting by varying the inerter property of the energy harvesting enabled TMDI. Finally, Section 6 summarizes the main conclusions of the work.

2. The tuned mass-damper-inerter for single-degree-of-freedom (SDOF) structures

2.1 Rack-and-pinion flywheel-based ideal inerter

The ideal inerter was conceptually defined by Smith (2002) as a linear two terminal mechanical element of negligible physical mass/weight developing an internal (resisting) force F proportional to the relative acceleration of its terminals. That is

$$F = b(\ddot{u}_1 - \ddot{u}_2) \quad (1)$$

where u_1 and u_2 are the displacement coordinates of the inerter terminals and, hereafter, a dot over a symbol denotes time differentiation. In the above equation, the constant of proportionality b is the so-called inertance measured in mass units (kg). Importantly, several different inerter prototypes were devised and experimentally characterized over the past decade achieving inertance values b orders of magnitude larger than the devices' physical mass, while approximating the linear behavior in Eq. (1) within a wide frequency range of practical interest (e.g., Papageorgiou and Smith 2005, Wang *et al.* 2011, Chuan *et al.* 2012, Swift *et al.* 2013, Gonzalez-Buelga *et al.* 2016, Hu *et al.* 2016). For example, the early and most widely-known inerter implementations incorporate rack-and-pinion or ball-screw mechanisms to transform, through gearing, the translational kinetic energy associated with the relative motion of the device terminals into rotational kinetic energy at a lightweight fast-spinning disk or "flywheel" (Smith 2002, Papageorgiou and Smith 2005). The inertance in such

flywheel-based inerters depends primarily on the number of gears and on the gearing ratio used to drive the flywheel, rather than on the mass of the flywheel.

To elaborate further on this point, consider a typical mechanical realisation of the inerter comprising a flywheel linked to a rack-and-pinion via n gears. Fig. 1 depicts such a device for the special case of $n=4$. The inertance of this device is given by

$$b = m_f \frac{\gamma_f^2}{\gamma_{pr}^2} \left(\prod_{k=1}^n \frac{r_k^2}{pr_k^2} \right) \quad (2)$$

where m_f and γ_f are the mass and the radius of gyration of the flywheel, respectively, γ_{pr} is the radius of the flywheel pinion, and r_k and pr_k ($k=1,2,\dots,n$) are the radii of the k -th gear and its corresponding pinion, respectively, linking the rack to the flywheel pinion (see also Fig. 1). Assuming a flywheel of 10kg mass with a ratio $\gamma_f / \gamma_{pr} = 3$ driven by a single gear (i.e., $n=1$) with a $r_1 / pr_1 = 4$ gear ratio, the inertance computed from Eq. (2) is $b = 1440$ kg (see also Smith 2002). Adding two more gears with a common gear ratio equal to 3, yields an inerter with $b = 116640$ kg, that is, a device with a physical mass three orders of magnitude smaller than its inertance. The above simple example illustrates the scalability of flywheel-based inerters through gearing. It also suggests that it is practically feasible to achieve inerters with adjustable/varying inertance without any change to their weight either in a stepped manner, by means of standard gearboxes with fixed gear ratios, or, continuously, by means of continuously varying transmission gearboxes, similar to those used in automotive engineering applications (Dhand and Pullen 2015).

In view of Eqs. (1) and (2), it is seen that the ideal (linear) inerter can be construed as an inertial/mass amplification device whose gain depends on b and on the relative acceleration observed by its terminals. In fact, in the special case where one of the inerter terminals is "grounded" (i.e., linked to a stationary point), the inerter behaves as a "weightless" mass equal to b . For instance, by setting \ddot{u}_2 in Eq. (1), the inertance b is added to the physical mass associated with the dynamic degree-of-freedom (DOF) corresponding to the displacement u_1 within a dynamical system.

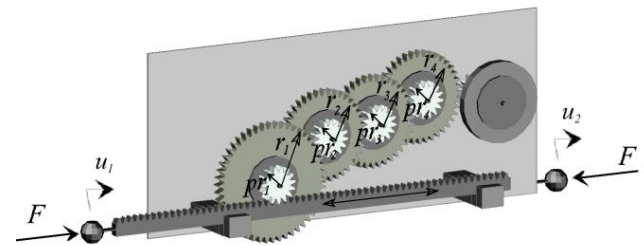


Fig. 1 Schematic representation of a rack-and-pinion flywheel-based inerter device with 4 gears

This inerter property was originally recognized by Smith (2002) and motivates the consideration of the so-called tuned mass-damper-inerter (TMDI) configuration (Marian and Giaralis 2014) reviewed in the following sub-section.

2.2 Equations of motion for TMDI equipped SDOF primary structures

Consider the class of dynamically excited structures amenable to be modelled as single-degree-of-freedom (SDOF) systems. The TMDI aims to suppress the motion of such systems (primary structures) by coupling the classical tuned mass-damper (TMD) with a grounded inerter in a skyhook configuration (Marian and Giaralis 2014). Specifically, the TMDI comprises a mass m_2 attached to the primary structure via a linear spring of stiffness k_2 and a viscous damper with damping coefficient c_2 , along with an inerter device with inertance b linking the attached mass to the ground as shown in Fig. 2. It is emphasized, in passing, that the TMDI is different from the various inerter-based DVAs considered by Hu and Chen (2015) and optimally designed in Hu *et al.* (2015) for harmonic excitation. In the latter DVAs, motivated mostly by suspension systems in vehicle engineering applications, the inerter is sandwiched in between the primary structure and the attached mass in conjunction with damper and spring elements in different layouts. Nevertheless, the TMDI considers a sky-hooked (grounded) inerter aiming to suppress vibrations in stationary (i.e., non-moving) primary structures. A practical example is the case of highway truss bridges oscillating along their longitudinal direction in which the deck is interpreted as the attached mass m_2 connected to the main truss of mass m_1 through bearings modelled via the spring k_2 and dashpot c_2 as considered by Hoang *et al.* (2008). In this case, the inerter can link the bridge deck to the ground at the abutments and the dynamical system of Fig.2 applies to find the optimal bearing system that would minimise the truss vibrations in the longitudinal direction of the bridge.

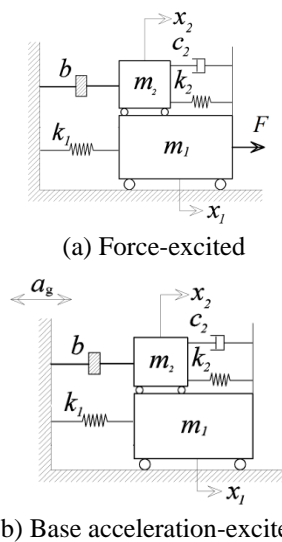


Fig. 2 Tuned mass-damper-inerter-equipped SDOF primary structure

The equations of motion of a TMDI equipped undamped SDOF primary structure with mass m_1 and stiffness k_1 are written in matrix form as

$$\begin{bmatrix} m_2 + b & 0 \\ 0 & m_1 \end{bmatrix} \begin{Bmatrix} \ddot{x}_2 \\ \ddot{x}_1 \end{Bmatrix} + \begin{bmatrix} c_2 & -c_2 \\ -c_2 & c_2 \end{bmatrix} \begin{Bmatrix} \dot{x}_2 \\ \dot{x}_1 \end{Bmatrix} + \begin{bmatrix} k_2 & -k_2 \\ -k_2 & k_1 + k_2 \end{bmatrix} \begin{Bmatrix} x_2 \\ x_1 \end{Bmatrix} = \begin{Bmatrix} F_2(t) \\ F_1(t) \end{Bmatrix} \quad (3)$$

under the assumption that the physical mass of the inerter, the damper, and the spring are negligible compared to the m_1 and m_2 masses. In the previous equations, x_1 and x_2 are the displacement response histories relative to the ground of the primary structure and of the attached mass, respectively. Furthermore, the forcing vector in the right hand size of Eq. (3) specializes as

$$\begin{Bmatrix} F_2(t) \\ F_1(t) \end{Bmatrix} = \begin{Bmatrix} 0 \\ F(t) \end{Bmatrix} \quad \text{or} \quad \begin{Bmatrix} F_2(t) \\ F_1(t) \end{Bmatrix} = -\begin{Bmatrix} m_2 \\ m_1 \end{Bmatrix} a_g(t) \quad (4)$$

The first vector in Eq. (4) corresponds to a force-excited primary structure subject to a load $F(t)$ as shown in Fig. 2(a). The second vector in Eq. (4) corresponds to a base-excited primary structure subject to the ground acceleration time-history $a_g(t)$ as shown in Fig. 2(b).

In view of Eqs. (3) and (4), it is readily seen that for the case of force-excited primary structures, the TMDI coincides with a classical TMD with attached mass $m_2 + b$. In this regard, all known approaches and formulae for vibration control and energy harvesting for force-excited SDOF primary structures equipped with the classical TMD are applicable for the TMDI as well: one needs only to replace the attached TMD mass, m_2 , by the sum of the attached mass and the inertance, $m_2 + b$, as required in the various expressions derived for the classical TMD (e.g., Den Hartog 1956, Krenk 2005, Salvi and Rizzi 2016). However, this is not the case for acceleration base-excited primary structures in which the effective (inertial) force applied to the attached mass due to the ground acceleration is proportional to m_2 and not to $m_2 + b$. To this end, only the case of acceleration base-excited TMDI equipped primary structures is explicitly considered in the ensuing mathematical development as the associated expressions quantifying the performance for vibration suppression and energy harvesting cannot be trivially derived by substitution to known results applicable to the classical TMD. Still, certain plots and final analytical formulae pertaining to force-excited TMDI equipped primary structures will also be presented and discussed in subsequent sections for the sake of completeness and comparison, as deemed essential.

Denote by ω_{TMDI} and ζ_{TMDI} the natural frequency and the critical damping ratio of the TMDI, respectively, defined as

$$\omega_{TMDI} = \sqrt{\frac{k_2}{m_2 + b}}, \quad \zeta_{TMDI} = \frac{c_2}{2(m_2 + b)\omega_{TMDI}} \quad (5)$$

Further, consider the mass ratio μ , frequency ratio ν_{TMDI} , and inertance ratio β expressed as

$$\mu = \frac{m_2}{m_1}, \quad \nu_{TMDI} = \frac{\omega_{TMDI}}{\omega_1}, \quad \text{and} \quad \beta = \frac{b}{m_1} \quad (6)$$

respectively, where $\omega_I = (k_I/m_I)^{1/2}$ is the natural frequency of the primary structure. Using the above dimensionless quantities, the complex frequency response function (FRF) in terms of the relative displacement x_I of the base-excited primary structure in Fig. 2(b) can be written as

$$G_1(\omega) = \frac{x_I}{a_g} \omega_I^2 = \frac{(1+\mu)\omega_{TMDI}^2 - \omega^2 + i2\zeta_{TMDI}(1+\mu)\omega_{TMDI}\omega}{\left(1 - \frac{\omega^2}{\omega_I^2}\right)(\omega_{TMDI}^2 - \omega^2 + i2\zeta_{TMDI}\omega_{TMDI}\omega) - \frac{\beta+\mu}{\omega_I^2}(\omega_{TMDI}^2 + i2\zeta_{TMDI}\omega_{TMDI}\omega)\omega^2} \quad (7)$$

in the domain of frequencies ω by considering the normalized acceleration input a_g/ω_I^2 . In the latter equation and hereafter $i = \sqrt{-1}$. Moreover, the complex FRF for the same dynamical system in terms of the relative displacement x_2 of the attached mass is written as

$$G_2(\omega) = \frac{x_2}{a_g} \omega_I^2 = \frac{(1+\mu)(\omega_{TMDI}^2 + i2\zeta_{TMDI}\omega_{TMDI}\omega) + \frac{\mu}{\beta+\mu}(\omega_I^2 - \omega^2)}{\left(1 - \frac{\omega^2}{\omega_I^2}\right)(\omega_{TMDI}^2 - \omega^2 + i2\zeta_{TMDI}\omega_{TMDI}\omega) - \frac{\beta+\mu}{\omega_I^2}(\omega_{TMDI}^2 + i2\zeta_{TMDI}\omega_{TMDI}\omega)\omega^2} \quad (8)$$

Note that by setting $b=\beta=0$ in Eqs. (7) and (8), the FRFs in terms of the relative displacements x_I and x_2 , respectively, for an undamped SDOF primary structure equipped with the classical TMD are retrieved. In this regard, the classical TMD may be viewed as a special case of the TMDI.

In the following section, optimal TMDI design for undamped harmonically excited SDOF primary structures is sought by considering the minimization of the peak value attained by the magnitude of the FRF in Eq. (7), $|G_1(\omega)|$, hereafter referred to as the dynamic amplification factor (DAF). This is the most common design criterion adopted in the literature for vibration suppression under harmonic excitation (Krenk 2005). Further, in Section 4, the kinetic energy of the TMDI equipped SDOF primary structures available to be transformed into electric energy via a standard electromagnetic energy harvester is quantified. The latter requires the consideration of both the FRFs in Eqs. (7) and (8).

3. Optimal TMDI design and performance for vibration suppression in harmonically excited SDOF structures

3.1 Derivation of TMDI parameters in closed-form based on the fixed point theory

Assume that the TMDI equipped structure in Fig. 2(b) is subjected to a harmonic ground acceleration excitation a_g . Given fixed values for the μ and β ratios defined in Eq. (6), it is sought to determine optimal values for the TMDI stiffness coefficient k_2 and damping coefficient c_2 , or, equivalently, for the dimensionless frequency and damping ratios ν_{TMDI} and ζ_{TMDI} defined in Eqs. (6) and (5), respectively, such that the peak relative displacement of the primary structure is minimized. To this aim, the optimal tuning/design approach of Den Hartog (1956) is herein

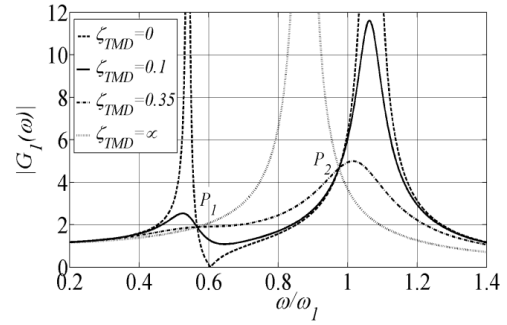


Fig. 3 Relative displacement response amplitude of undamped support excited TMDI equipped SDOF primary structure with mass ratio $\mu=0.1$, inertance ratio $\beta=0.1$, frequency ratio $\nu_{TMDI}=0.5$, and for various damping ratios ζ_{TMDI}

adopted. This approach is based on the “fixed point theory” which relies on the empirical observation that the DAF curves $|G_1(\omega)|$ in Eq. (7) for $b=\beta=0$ (i.e., for the classical TMD) and for fixed attached mass and frequency ratio pass through two specific points, the location of which is independent of the damping coefficient c_2 . Importantly, this observation holds for TMDI equipped harmonically base-excited primary structures (case of $\beta \neq 0$), as well. For illustration, Fig. 3 plots the DAF $|G_1(\omega)|$ in Eq. (7) for several values of the TMDI damping ratio ζ_{TMDI} and for fixed values μ , β , and ν_{TMDI} . Evidently, there exist two “stationary” points, denoted by P_1 and P_2 , where the DAF curves intersect for all damping coefficient values c_2 or, equivalently, for all TMDI damping ratios ζ_{TMDI} .

The location of P_1 and P_2 points on the frequency axis can be found by considering the equation

$$\lim_{\zeta_{TMDI} \rightarrow \infty} |G_1(\omega)|^2 = \lim_{\zeta_{TMDI} \rightarrow 0} |G_1(\omega)|^2 \quad (9)$$

By collecting the real and imaginary parts in the numerator and denominator in Eq. (7), the square magnitude of the FRF $G_1(\omega)$ can be expressed as

$$|G_1(\omega)|^2 = \frac{A^2 + 4\zeta_{TMDI}^2 B^2}{C^2 + 4\zeta_{TMDI}^2 D^2} \quad (10)$$

where

$$\begin{aligned} A &= (1+\mu)\omega_{TMDI}^2 - \omega^2, \quad B = (1+\mu)\omega_{TMDI}\omega, \\ C &= \frac{\omega^4}{\omega_I^2} - \omega^2 \left[1 + \frac{\omega_{TMDI}^2}{\omega_I^2} (1+\beta+\mu) \right] + \omega_{TMDI}^2, \quad \text{and} \\ D &= \omega\omega_{TMDI} \left[1 - \frac{\omega^2}{\omega_I^2} (1+\beta+\mu) \right]. \end{aligned} \quad (11)$$

By substituting Eq. (10) in Eq. (9) and upon some algebraic manipulation, one obtains

$$AD = \pm BC \quad (12)$$

Adopting the positive sign in Eq. (12) and making use of the expressions in Eq. (11), the trivial (static) solution $\omega=0$ is reached, which is not of interest. However, by

adopting the negative sign in Eq. (12) together with Eq. (11) yields the following quadratic equation in ω^2

$$(2\mu + \beta + 2)\omega^4 - [\omega_1^2(2 + \mu) + 2\omega_{TMDI}^2(1 + \beta + \mu)(1 + \mu)]\omega^2 + 2(1 + \mu)\omega_1^2\omega_{TMDI}^2 = 0 \quad (13)$$

The two roots, ω_{P1}^2 and ω_{P2}^2 , of the last equation are the squared frequencies corresponding to the stationary points P_1 and P_2 .

The tuning approach of Den Hartog (1956) suggests that the peak response of the considered primary structure is minimized when the following two conditions hold:

- (I) $|G_I(\omega)|$ attains the same value at the points P_1 and P_2 , and
- (II) $|G_I(\omega)|$ attains a local maximum at the points P_1 and P_2 .

By enforcing condition (I) for the limiting value $\zeta_{TMDI} \rightarrow \infty$, that is

$$\lim_{\zeta_{TMDI} \rightarrow \infty} |G_I(\omega_{P1})| = \lim_{\zeta_{TMDI} \rightarrow \infty} |G_I(\omega_{P2})| \quad (14)$$

the following expression for the sum of the roots of Eq. (13) is reached

$$\omega_{P1}^2 + \omega_{P2}^2 = \frac{2\omega_1^2}{1 + \beta + \mu} \quad (15)$$

Further, a second expression for the sum of the roots of Eq. (13) can be readily written as

$$\omega_{P1}^2 + \omega_{P2}^2 = \frac{\omega_1^2(2 + \mu) + 2\omega_{TMDI}^2(1 + \beta + \mu)(1 + \mu)}{(2\mu + \beta + 2)} \quad (16)$$

This is obtained by taking the ratio of the linear coefficient over the quadratic coefficient in Eq. (13) with the negative sign. Making use of Eqs. (15) and (16) the following formula for the optimal frequency ratio in Eq. (6) is obtained in closed-form as a function of the (given) ratios μ and β

$$\nu_{TMDI}^{OPT} = \frac{1}{1 + \beta + \mu} \sqrt{\frac{(1 + \mu)(2 - \mu) - \mu\beta}{2(1 + \mu)}} \quad (17)$$

The above frequency ratio ensures that $|G_I(\omega)|$ in Eq. (7) attains the same value at frequencies ω_{P1} and ω_{P2} for any ζ_{TMDI} since it satisfies condition (I) through Eq. (14).

Next, condition (II) of the Den Hartog design approach is enforced by setting the first derivative of $|G_I(\omega)|$ at the two stationary points equal to zero. That is

$$\left. \frac{d|G_I(\omega)|}{d\omega} \right|_{\omega=\omega_{P1}} = \left. \frac{d|G_I(\omega)|}{d\omega} \right|_{\omega=\omega_{P2}} = 0 \quad (18)$$

Application of Eq. (18) yields two *different* values for ζ_{TMDI} which make the gradient of the DAF curve zero at the two stationary points. Following Brock (1946), the “optimal” TMDI parameter ζ_{TMDI} is taken as the average of these two values (though other alternatives are possible Krenk (2005)), yielding

$$\zeta_{TMDI}^{OPT} = \sqrt{\frac{\beta^2\mu + 6\mu(1 + \mu)^2 + \beta(1 + \mu)(6 + 7\mu)}{8(1 + \mu)(1 + \beta + \mu)[2 + \mu(1 - \beta - \mu)]}} \quad (19)$$

Substituting in Eq. (7) the TMDI tuning parameters in Eqs. (17) and (19), the following expression for the DAF at points P_1 and P_2 is reached

$$\max_{\omega} \{|G_I(\omega)|\} = |G_I(\omega_{P1})| = |G_I(\omega_{P2})| = \sqrt{\frac{(1 + \mu)(\beta + 2\mu + 2)}{\beta + \mu}} \quad (20)$$

Note that by setting $\beta=b=0$ to Eqs. (17), (19) and (20) the closed-form expressions for optimal parameters and DAF of the classical TMD for undamped harmonic base acceleration excited SDOF systems are retrieved (Warburton 1982). In the remainder of this section, the potential of the TMDI vis-à-vis the classical TMD to achieve enhanced vibration suppression for the same attached mass and attached mass/weight reduction for the same level of vibration suppression is assessed. In doing so, pertinent plots based on the herein considered optimal design approach are provided and discussed.

3.2 Vibration suppression performance of TMDI vis-à-vis the classical TMD

To facilitate a comparison between the TMDI configuration of Fig. 2(b) and the classical TMD, Table 1 collects the previously derived formulae for the optimal TMDI tuning parameters and the corresponding peak DAF for undamped SDOF primary structures subjected harmonic base acceleration with the known formulae for the classical TMD ($b=0$). Furthermore, closed-form expressions for optimal tuning parameters and peak DAF for the case of TMDI-equipped force excited primary structures (Fig. 2(a)) are also included in Table 1 for the sake of completeness. In the latter case, the expressions for the TMDI are trivially derived from the known expressions of the classical TMD (also included in Table 1) with attached mass m_2+b .

Further, Figs. 4(a) and 4(b) plot the optimal design parameters in Eqs. (17) and (19), respectively, for several different values of the mass ratio μ as a function of the inertance ratio β . The latter quantity takes values within a suggested interval of practical interest $[0,1]$, with $\beta=0$ being the limiting value for which the TMDI degenerates to the classical TMD. It is observed that the optimal frequency ratio ν_{TMDI} decreases as β increases for all values of μ considered, while it also decreases as the attached m_2 mass increases. Further, the optimum damping ratio ζ_{TMDI} increases monotonically with the normalized inerter constant β for all considered values of μ , while it also increases as the attached m_2 mass increases. The rate of change of both the TMDI optimum parameters with β is higher for smaller values of β and μ , while for $\mu>0.2$ the rate of change is almost constant. Similar trends are observed for the optimal parameters for the case of force-excited primary structures in Figs. 4(c) and 4(d), though a more prominent trend of saturation (i.e., decrease rate of

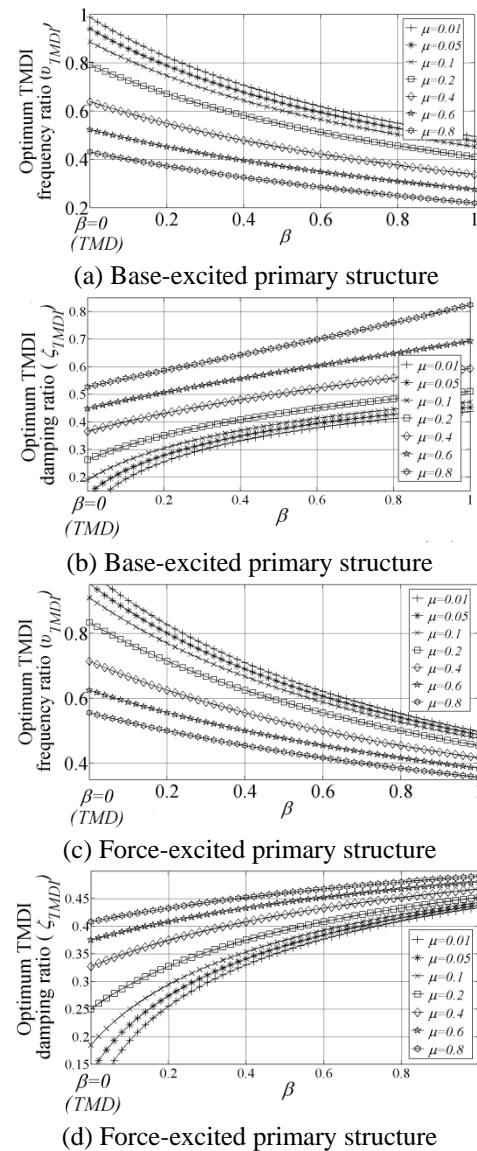
Table 1 Closed-form expressions for optimally tuned TMDI and classical TMD for undamped SDOF structures subjected to harmonic excitation

	Optimal frequency ratio (v_{TMDI})	Optimal damping ratio (ζ_{TMDI})	Peak dynamic amplification factor ($\max_{\omega} \{ G_1(\omega) \}$)
Force excited TMD*	$\frac{1}{1+\mu}$	$\sqrt{\frac{3\mu}{8(1+\mu)}}$	$\sqrt{\frac{2+\mu}{\mu}}$
Force excited TMDI	$\frac{1}{1+\beta+\mu}$	$\sqrt{\frac{3(\mu+\beta)}{8(1+\mu+\beta)}}$	$\sqrt{\frac{2+\mu+\beta}{\mu+\beta}}$
Base excited TMD**	$\frac{1}{1+\mu} \sqrt{\frac{2-\mu}{2}}$	$\sqrt{\frac{3\mu}{8(1+\mu)(1-\mu/2)}}$	$(1+\mu) \sqrt{\frac{2}{\mu}}$
Base excited TMDI	$\frac{1}{1+\beta+\mu} \sqrt{\frac{(1+\mu)(2-\mu)-\mu\beta}{2(1+\mu)}}$	$\sqrt{\frac{\beta^2\mu+6\mu(1+\mu)^2+\beta(1+\mu)(6+7\mu)}{8(1+\mu)(1+\beta+\mu)[2+\mu(1-\beta-\mu)]}}$	$\sqrt{\frac{(1+\mu)(\beta+2\mu+2)}{\beta+\mu}}$

* Den Hartog (1956); ** Warburton (1982)

change) is seen with β , especially for the relatively small values of mass ratio considered. A comparison between Figs. 4(a) and 4(b), and figs. 4(c) and 4(d), respectively, suggests that for $\mu < 0.1$ the optimal TMDI parameters are practically the same for the force-excited and the base-acceleration-excited primary structures across the considered range [0 1] of β values, despite the differences in the derived analytical formulae in Table 1. This observation suggests that β and μ ratios are not interchangeable in treating different types of excitations for relatively large attached mass ratios.

To assess the achieved level of vibration suppression by the TMDI vis-à-vis a same-weight classical TMD, Fig. 5(a) plots the DAF $|G_1(\omega)|$ for optimally designed (i.e., using the formulae in Table 1) TMDI-equipped undamped SDOF primary structure under harmonic base acceleration excitation with mass ratio $\mu = 0.1$ and for different values of the inertance ratio β , including the $\beta = 0$ value corresponding to the classical TMD. The frequency axis is normalized by the natural frequency of the uncontrolled primary structure ω_1 . It is seen that the larger the inertance of the optimally designed TMDI is, the more significant DAF reduction is achieved compared to the TMD case at the natural frequency ω_1 of the primary structure as well as at the frequencies ω_{p1} and ω_{p2} of the stationary points. Note, however, that as the inertance increases, the location of the stationary points shifts to lower frequencies and the distance of the two points increases. As a result, the DAF values for relatively low excitation frequencies (i.e., lower than 70% the resonant frequency ω_1) may increase with increasing inertance. Nevertheless, in practical applications, dynamic vibration absorbers are used to suppress excessive oscillations in harmonically excited structures due to resonance and, therefore, their vibration suppression performance is normally gauged within a relatively narrow frequency band centered at the natural frequency of the uncontrolled structure. In this regard, it is observed that optimally designed TMDIs perform remarkably better than a same-weight optimally designed TMD within a substantially wide frequency (wider than $[0.8\omega_1 \ 1.2\omega_1]$ for the considered case of $\mu = 0.1$) and, more importantly, the

Fig. 4 Optimum TMDI frequency ratio v_{TMDI} and damping ratio ζ_{TMDI} for varying inertance ratio β and for several mass ratio values μ for undamped SDOF primary structures

DAF curves become flatter across frequencies as the inertance ratio increases. The latter observation demonstrates that TMDIs with larger inertance ratios are also *more robust to detuning effects and to uncertainty* in the excitation frequency and/or in the primary structure properties than a same-weight TMD.

In light of the above discussion and plots in Fig. 5(a), it can be intuitively argued that an increase of the inertance in the TMDI has the same positive effects as an increase of the mass ratio in the TMD (see e.g., De Angelis *et al.* 2014), without, however, any substantial increase to the overall weight. To further elaborate on this important practical aspect, Fig. 5(b) plots DAF curves for optimally designed TMDs for different attached mass values. A comparison between Figs. 5(a) and 5(b) establishes that better vibration suppression close to resonance and increased robustness to detuning effects and uncertainty can be achieved either by increasing the attached mass (and therefore the added weight) of the classical TMD or by increasing the inertance of the TMDI (for a fixed attached mass/weight). Interestingly, for base acceleration excited primary structures (i.e., the case considered in Fig. 5) an optimally designed TMD with attached mass ratio μ_{TMD} performs worse than an optimally designed TMDI having a sum of the attached mass and inertance ratio, $\mu_{TMDI} + \beta$ equal to μ_{TMD} . Nevertheless, for force excited primary structures the previous two dynamic vibration absorbers yield the same DAF curve.

Further to the above comments, it is observed in Fig. 5(a) that the positive influence of the inerter tends to saturate with increasing inertance values. To better quantify this trend, Fig. 6 plots the peak DAF (i.e., $\max_{\omega} \{|G_1(\omega)|\}$ in

Table 1) for optimally designed TMDIs as a function of the inertance ratio β and for several attached mass ratios normalized by the peak DAF for optimally designed TMDs.

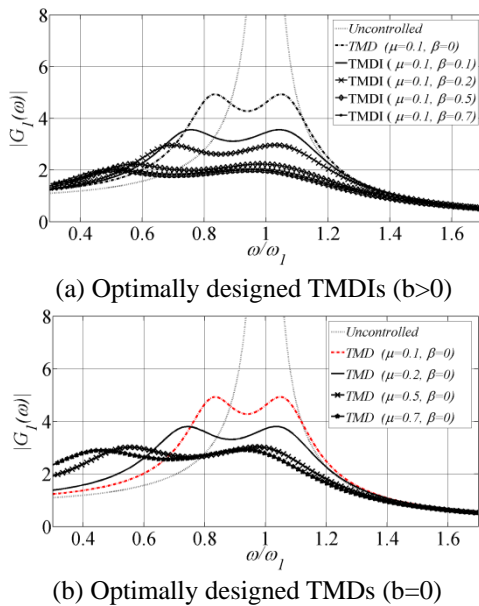


Fig. 5 Dynamic amplification factor (DAF) spectra for base acceleration excited primary structures

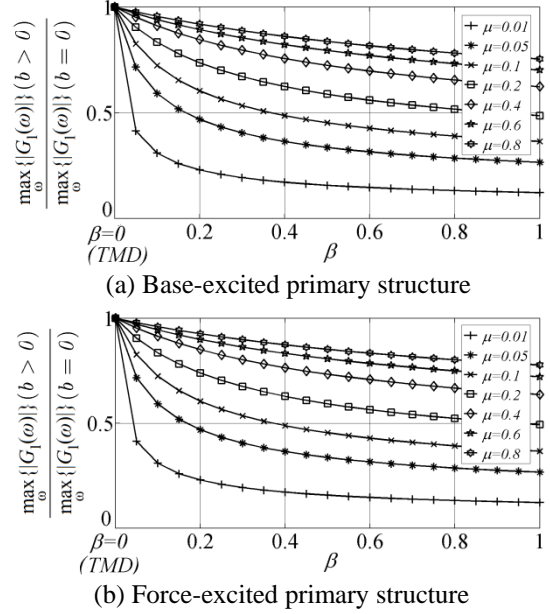


Fig. 6 Peak DAF of optimally designed TMDI-equipped SDOF structures normalized by the peak DAF of optimally designed TMD-equipped SDOF structures

It is seen that the rate of reduction of the peak DAF achieved by the TMDI compared to same-weight TMDs at the stationary points (note that the location of these points varies for each structure, since ω_{p1} and ω_{p2} frequencies are functions of μ and β as seen by Eqs. (13) and (17)), reduces as larger inertance ratio values are considered.

Furthermore, it is also deduced from Fig. 6 that for a fixed value of inertance the positive impact of the inerter is more prominent as TMDs with smaller attached mass are considered. In other words, the positive influence of increasing the attached TMDI mass saturates for larger mass ratios, as in the case of the classical TMD (see also Fig. 5(b)). The practical significance of this observation is that the inerter is more effective/beneficial for vibration suppression when it is coupled with more lightweight TMDs. Importantly, similar observations and trends on the improved level of vibration suppression achieved by the TMDI vis-a-vis the classical TMD as a function of the attached mass and inertance ratio hold for randomly base-excited primary structures (Marian and Giaralis 2014). As a final remark, the curves in Figs. 6(a) (base acceleration excitation) and 6(b) (force excitation) practically coincide even for excessively large attached mass ratio values.

3.3 Attached mass/weight reduction of TMDI vis-à-vis the classical TMD

The previous discussion quantified the improved vibration suppression capabilities of the TMDI vis-à-vis the classical TMD in a performance-assessment context. However, the TMDI bears a significant advantage over the TMD within the more practical performance-based design context: it achieves the same level of vibration suppression with significantly smaller attached mass ratios than the

classical TMD and therefore with significantly reduced added weight to a given primary structure. This aspect is quantified in Fig. 7 which plots the peak DAF in a TMD(I) design bar-chart format. These design charts provide for the required attached mass ratio to achieve a *target* (i.e., pre-specified by the design engineer) peak DAF for different values of inertance including the limiting case of $\beta=b=0$ corresponding to the classical TMD. For illustration, suppose that it is sought to achieve a peak DAF of 4 for a particular base acceleration excited primary structure. From Fig. 7(a), it is seen that this value of DAF can be achieved by an optimally designed TMDI with 60% smaller attached mass than the one required by an optimally designed classical TMD and an inertance ratio of $\beta=0.05$. Further, an optimally designed TMDI with double the previous inertance (i.e., $\beta=0.1$) achieves the target peak DAF of 4 with a 4.5 times smaller attached mass than the one required by the TMD yielding an overall significantly lighter dynamic vibration absorber. To further support this argument, assume that the mass of the primary structure under consideration is $m_1 = 360t$. A flywheel-based rack-and-pinion inerter with inertance $b = 36t$ (i.e., corresponding to $\beta=0.1$) can be achieved by using a flywheel with mass equal to 10kg and ratio $\gamma_f/\gamma_{pr} = 3$ connected to the rack by two gears ($n=2$ in Eq. (2)) with transmission ratios: $r_1/pr_1 = 5$ and $r_2/pr_2 = 4$ (see also Fig. 1). Clearly, the total weight of such an inerter device is negligible compared to the achieved inertance b .

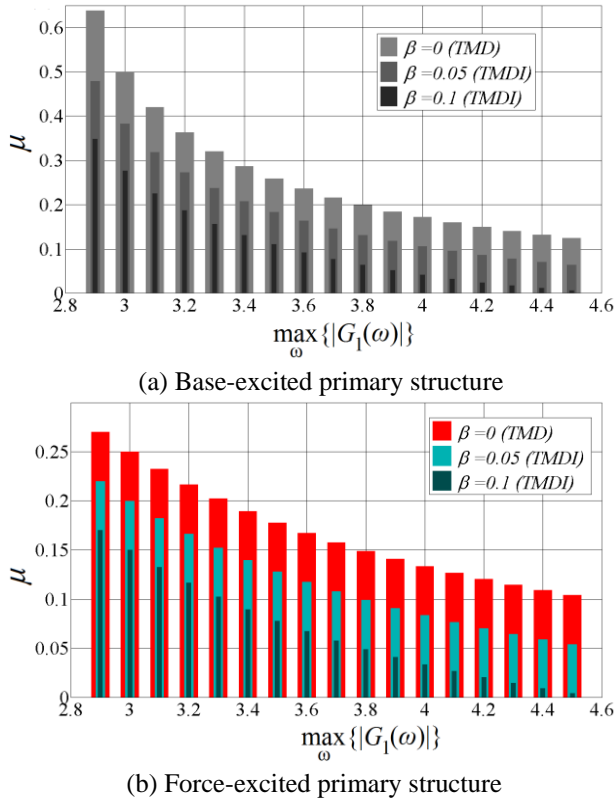


Fig. 7 Mass ratio against peak DAF bar-charts for optimum design of TMDI-equipped SDOF structures

4. Energy harvesting in harmonically excited TMDI equipped structures

4.1 An energy harvesting enabled TMDI

Having established the benefits of the TMDI for vibration suppression, this section explores its potential for harvesting energy from primary structure oscillations. To this aim, the linear dissipative damper of the TMDI is substituted by a linear translational electromagnetic motor (EM) shunted by a purely resistive load, as shown in Fig. 8. Compared to the standard TMD-based energy harvesters proposed in the literature for electric generation from low-frequency large-amplitude oscillations (see e.g., Tang and Zuo 2012, Gonzalez-Buelga *et al.* 2014), the herein considered energy harvesting-enabled TMDI considers additionally a grounded inerter. This consideration enables leveraging the inertia of the attached mass, without changing the DVA total weight. In this respect, the functionality of the inerter in the proposed configuration is significantly different from the various energy harvesters found in the literature which utilize rack-and-pinion (e.g., Tang and Zuo 2012) or ball-screw mechanisms (e.g., Cassidy *et al.* 2011, Hendijanizadeh *et al.* 2013), similar to those used in flywheel-based inerters, to enable the use of rotational EMs by transforming the translational kinetic energy to rotational kinetic energy.

The dashpot with coefficient c_M shown in the mechanical configurations of Fig. 8 is included to model the mechanical parasitic damping leading to energy losses. A standard EM comprising a moving magnet DC voice coil linear actuator is assumed (e.g., Zhu *et al.* 2012, Gonzalez-Buelga *et al.* 2014). The moving magnet observes the relative motion of the primary structure and of the attached mass and travels within a magnetic field of constant flux density J generating a voltage V expressed as

$$V = J(\dot{x}_1 - \dot{x}_2) \quad (21)$$

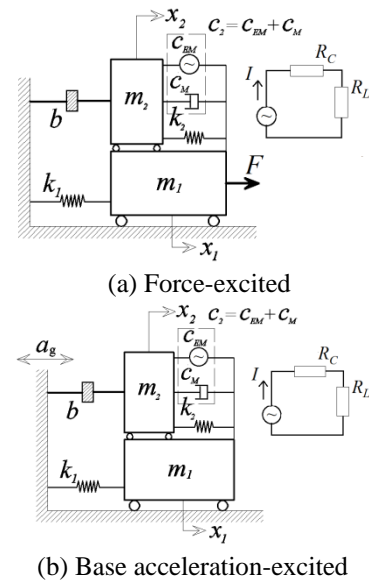


Fig. 8 Energy harvesting enabled TMDI-equipped SDOF primary structure

The EM resists the relative motion between the primary structure and the attached mass by developing a damping force F_{EM} in the mechanical domain written as

$$F_{EM} = c_{EM} (\dot{x}_1 - \dot{x}_2) \quad (22)$$

where c_{EM} is the electromechanical damping coefficient. The above damping force is linearly proportional to the generated electric current I , that is

$$F_{EM} = J I \quad (23)$$

Using Eqs. (21) to (23) in conjunction with Ohm's law $I=V/R$, which relates the electric current I through a circuit with total resistance R due to a voltage V , the electromechanical damping coefficient c_{EM} is expressed as

$$c_{EM} = \frac{J^2}{(R_C + R_L)} \quad (24)$$

In the last equation, R_C represents the internal "parasitic" resistance of the EM modeling the energy losses within the device, while R_L is the resistive load. In deriving Eq. (24), the inductance of the EM is neglected (e.g., Zhu *et al.* 2012). A comparison between the dynamical systems in Figs. 2 and 8 suggests that the equations of motion and the FRFs of section 2.2 are applicable to the herein considered energy harvesting enabled TMDI by setting

$$c_2 = c_{EM} + c_M \quad (25)$$

4.2 Quantification of the available energy for harvesting

In this section, the available energy to be harvested from the vibrating system of Fig. 8 is quantified by assuming that the energy harvesting enabled TMDI is optimally designed for vibration suppression under harmonic excitation as detailed in section 3.1. (Table 1). Specifically, the available power to be harvested through the resistive load R_L is given by the standard relationship in the electrical domain

$$P = I^2 R_L \quad (26)$$

Using the above relationship in conjunction with Eq. (21) and Ohm's law, the following expression for the available power to be harvested from the dynamical systems in Fig. 8 under harmonic excitation is reached

$$P(\omega) = \frac{J^2}{(R_C + R_L)^2} |G_{RV}(\omega)|^2 R_L \quad (27)$$

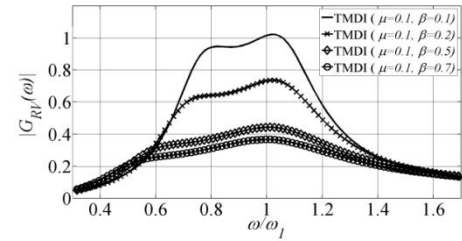
In the above equation, G_{RV} is the relative velocity FRF between the m_1 mass of the primary structure and the attached m_2 mass given as

$$G_{RV}(\omega) = i\omega \frac{G_1(\omega) - G_2(\omega)}{\omega_1^2} \quad (28)$$

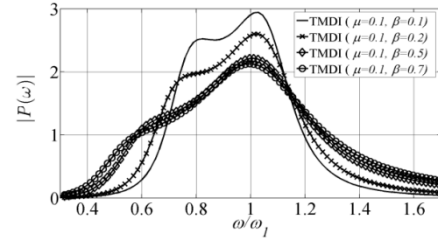
where the FRFs G_1 and G_2 have been defined in Eqs. (7) and (8), respectively, for base acceleration excitation.

Similar expressions for G_1 and G_2 readily follow from Eqs. (3) and (4) for force excited primary structures.

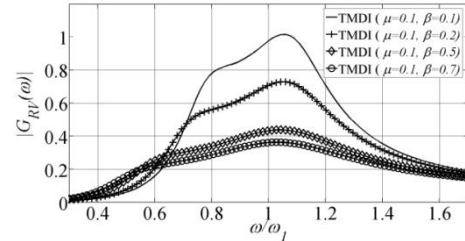
Figs. 9(a) and 9(c) plot the magnitude of the G_{RV} FRFs against the normalized frequency by $\omega/\omega_1 = (k_1/m_1)^{1/2}$ for optimally designed TMDI-equipped undamped SDOF primary structures under base acceleration and force excitations, respectively, with mass ratio $\mu = 0.1$ and for different values of the inertance ratio β . It is seen that the values of these FRF spectra reduce for increasing inertance ratios which achieve an overall improved level of vibration suppression (see also Figs. 5(a) and 6). However, the reduction of $|G_{RV}|$ is not beneficial in terms of energy harvesting as is readily seen in Eq. (27). The effect of the increased inertance ratio β to the energy harvesting potential of the proposed TMDI system is quantified in Figs. 9(b) and 9(d) plotting the magnitude of the power in Eq. (27) as a function of the normalized ω/ω_1 frequency.



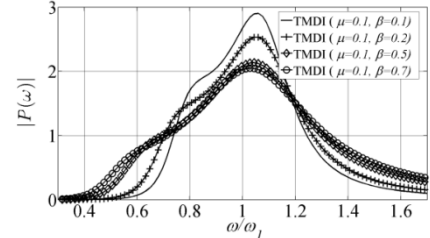
(a) Base-excited primary structure



(b) Base-excited primary structure



(c) Force-excited primary structure



(d) Force-excited primary structure

Fig. 9 Relative velocity amplitude FRF (Eq. (28)) and available power for harvesting (Eq. (29)) spectra for various optimally designed TMDI equipped SDOF primary structures

These plots have been obtained by taking $J=11.34$ N/A and $R_c=2.96\Omega$ which corresponds to a particular off-the-shelf EM device used by Gonzalez-Buelga *et al* (2014), and by assuming that $c_M = c_{EM}$. It is observed that the increase of the ratio β reduces the available power for harvesting close to the natural period of the primary structure. However, similarly to what has been observed and discussed in view of Fig. 5(a), the effect of β to saturates for $\beta>0.5$, while the range of frequencies that the available power spectra take on non-negligible values increases (i.e., the curves become flatter). In every case, by juxtaposing Figs. 5(a) and 9(b), the well-known trade-off between vibration suppression performance and available energy for harvesting of the TMD-based energy harvesters (e.g., Tang and Zuo 2012, Ali and Adhikari 2013 and Gonzalez-Buelga *et al.* 2014) is confirmed for the proposed energy harvesting enabled TMDI, as well. In passive optimally designed TMD-based energy harvesters, this trade-off depends heavily on the assumed TMD inertial property governed by the fixed mass ratio μ (e.g., Gonzalez-Buelga *et al.* 2014). Nevertheless, the inertial property of the herein considered TMDI system, depends not only on the *a priori* fixed mass ratio μ , but also on the inertance ratio β . To this end, the next section explores the potential of considering passive sub-optimal TMDIs with varying inertance to achieve increased available energy for electric power generation.

5. Enhanced energy harvesting TMDI performance through varying inertance

In certain practical applications, it may be desired to increase electric power generation from primary structure oscillations during times when vibration suppression requirements are relaxed. In conventional TMD-based energy harvesters, such considerations are addressed by varying the damping property of the EM (e.g., Cassidy *et al.* 2011, Zhu *et al.* 2012, Gonzalez-Buelga *et al.* 2014), to achieve a desirable trade-off between energy harvesting and vibration suppression. However, in the case of the energy harvesting enabled TMDI of Fig. 8 it is viable to achieve a trading between the above two objectives by varying its total apparent inertia, intuitively defined as m_2+b . This can be accomplished by considering a typical flywheel-based inerter, as the one shown schematically in Fig. 1, with varying inertance b in Eq. (2) via standard transmission gearboxes to switch gearing ratios r_k / pr_k and/or the number of gearing stages n .

To illustrate the usefulness of treating the inertance property of the energy harvesting-enabled TMDI as a “degree of freedom” leveraging the trade-off between energy harvesting and vibration suppression, Fig. 10 plots DAF spectra and available power for harvesting spectra for one optimally designed TMDI for vibration suppression with mass ratio $\mu=0.1$ and inertance ratio $\beta=0.6$ and for several sub-optimal TMDIs. The optimal TMDI parameters are determined as $v_{TMDI}^{OPT}(\mu=0.1, \beta=0.6)=0.5651$ and $\zeta_{TMDI}^{OPT}(\mu=0.1, \beta=0.6)=0.4132$ using Eqs. (17) and (19), respectively. It is observed that as β reduces, the (sub-

optimal) TMDI allows for more energy to be harvested across a range of excitation frequencies centered at the primary structure natural frequency ω_1 , at the cost of increased oscillations to the primary structure at the same range of frequencies. Therefore, by keeping constant all the TMDI properties but the inertance b leverages effectively the trade-off between energy harvesting and vibration suppression. This aspect is further quantified in Fig. 11 which plots the normalized peak DAF and peak available power for harvesting for non-optimal TMDIs as the inertance ratio β changes for four different values of the mass ratio μ and for constant optimal TMDI parameters ($\beta=0.6$) reported in Table 2. As the inertance is reduced below $\beta=0.6$ (i.e., departing from the optimum design point for vibration control), the available energy for harvesting increases significantly (for fixed attached mass, stiffness, and damping properties).

It is important to note that in the above presented numerical results and discussion the damping and stiffness properties of the TMDI are purposely kept constant, for the following two reasons: (i) to isolate the effect of a varying inertance to the achieved levels of vibration suppression and of available energy for harvesting, and (ii) to by-pass the need of posing any particular, and therefore non-general, optimization criterion balancing between the conflicting objectives of minimizing the oscillation amplitude of the primary structure and maximizing energy generation. Nevertheless, it is possible to vary the stiffness and/or the damping properties, as well, to achieve an overall optimal retuning of the device assembly as a whole, yet such considerations fall outside the scope of this study and are left for future work.

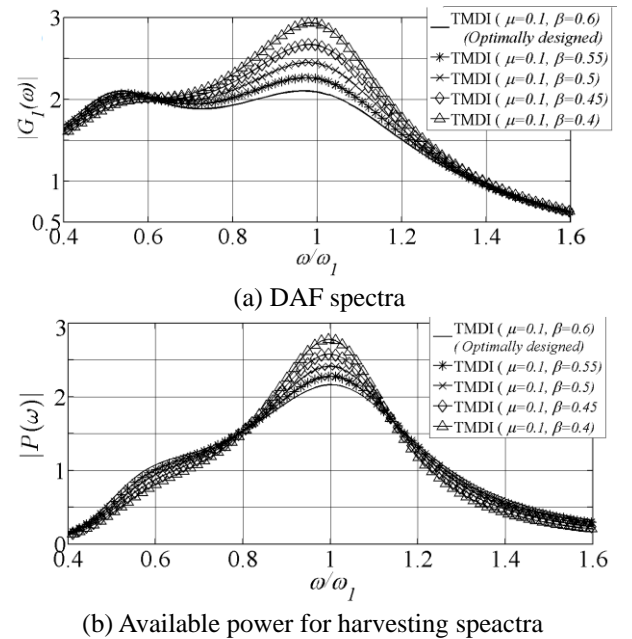
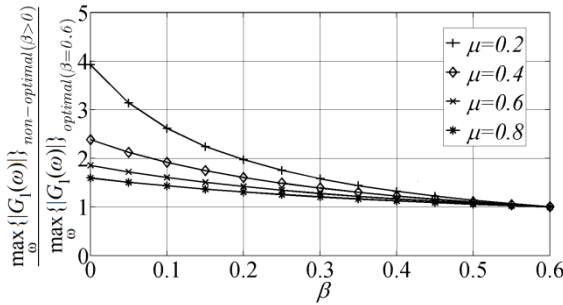


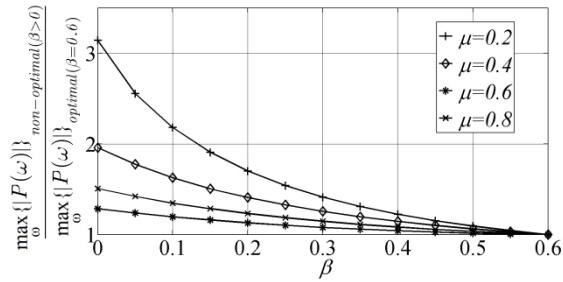
Fig. 10 Performance of optimally designed TMDI system for vibration suppression with $\mu=0.1$ and $\beta=0.6$ (constant $v_{TMDI}=0.5651$ and $\zeta_{TMDI}=0.4132$) and for several values of inertance

Table 2 Optimal TMDI parameters derived for $\beta=0.6$ and several mass ratio μ values

Mass ratio μ	Frequency ratio	ζ_{TMDI}^{OPT}	Damping ratio	ζ_{TMDI}^{OPT}
0.2	0.5512		0.4497	
0.4	0.4226		0.5227	
0.6	0.3484		0.6026	
0.8	0.2846		0.6990	



(a) Peak DAF



(b) Peak available power for harvesting

Fig. 11 Performance of *non-optimal* TMDIs normalized by the peak DAF and peak available power for harvesting, respectively for optimally designed TMDI for $\beta=0.6$ as functions of the inertia ratio β

6. Conclusions

The TMDI configuration, recently introduced by the authors for vibration suppression of stochastically base-excited structures, have been considered for vibration control and energy harvesting in harmonically excited structures. Closed-form analytical expressions for optimal TMDI parameters, stiffness and damping, given mass and inertance ratios have been derived by application of Den Hartog semi-empirical approach widely used for the design of the classical TMD to suppress the motion of harmonically excited undamped SDOF structures. Based on pertinent analytically derived results, it was shown that the TMDI is more effective from a same mass/weight classical TMD to suppress vibrations close to the natural frequency of the uncontrolled structure, while it is more robust to detuning effects and uncertainties in estimating the structural properties of the primary structure. This is because the TMDI exploits the mass amplification effect of a grounded inerter: the larger the inerter constant (inertance), the more reduction to the peak response displacement of the primary structure is achieved over a wider band of frequencies for

the same attached mass. Moreover, it was demonstrated that the mass amplification effect of the inerter coupled with the herein derived optimum TMDI design parameters achieves significant weight reductions for a target/predefined level of vibration suppression in the context of performance-based design compared to the classical TMD. It is expected that this aspect of the TMDI can lead to simple and cost-effective robust vibration suppression in demanding practical applications enjoying many practical benefits over large-mass passive TMDs. Furthermore, the potential of simultaneous energy harvesting and vibration suppression in passive mode by means of a novel energy harvesting enabled TMDI has been explored utilizing a typical electromagnetic motor for electric energy generation. It was shown that the inertance leverages the available power to be harvested in an optimally designed TMDI for vibration suppression. This was achieved by treating the inertance as an inertial/mass related degree of freedom, not normally considered in the design of conventional TMDs for energy harvesting, assuming the availability of a flywheel-based inerter device implementation with varying inertance through mechanical gearing.

Overall, the herein furnished analytical results have quantified the benefits of coupling a grounded linear inerter device with the classical TMD for vibrations suppression, attached weight reduction, and energy harvesting in harmonically excited SDOF structures. In this respect, it is envisioned that this study will pave the way for further developments, through theoretical and experimental research, towards adaptive DVAs and energy harvesters with varying inertial/mass properties, besides stiffness and damping, yielding smart structures and structural components. Nevertheless, further research is warranted to gauge the gains of the TMDI over the classical TMD in terms of weight reduction and energy harvesting in multi-mode MDOF structures such as in wind-excited tall buildings. In such structures, the TMDI mass is attached towards the top floors via dampers and linear stiffeners, or hangers in case of pendulum-like TMD implementations and, therefore, the inerter cannot be grounded: it needs to be connected to a different floor from the one that the mass damper is attached to (Marian and Giaralis 2014, Giaralis and Petrini 2017).

Acknowledgements

The first author gratefully acknowledges the support of City, University of London through a PhD studentship. The second author is thankful to the financial support of EPSRC in UK, under grant EP/M017621/1.

References

- Adhikari, S. and Ali, F. (2013), "Energy harvesting dynamic vibration absorbers", *J. Appl. Mech.*, **80**(4), 1-9.
- Asami, T., Nishihara, O. and Baz, A.M. (2002), "Analytical solutions to H_∞ and H_2 optimization of dynamic vibration absorber attached to damped linear systems", *J. Vib. Acoust.*, **124**(2), 284-295.

- Bakre, S.V. and Jangid, R.S. (2007), "Optimum parameters of tuned mass damper for damped main system", *Struct. Control Health Monit.*, **14**(3), 448-470.
- Bandivadekar, T.B. and Jangid, R.S. (2012), "Mass distribution of multiple tuned mass dampers for vibration control of structures", *Int. J. Civil Struct. Eng.* **3**, 70-84.
- Bortoluzzi, D., Casciati, S., Elia, L. and Faravelli, L. (2015), "Design of a TMD solution to mitigate wind-induced local vibrations in an existing timber footbridge", *Smart Struct. Syst.*, **16**(3), 459-478.
- Brock, J.E. (1946), "A note on the damped vibration absorber", *J. Appl. Mech.*, **13**, A-284.
- Casciati, F. and Giuliano, F. (2009), "Performance of multi-TMD in the towers of suspension bridges", *J. Vib. Control*, **15**(6), 821-847.
- Cassidy, I.L., Scruggs, J.T., Behrens, S. and Gavin, H.P. (2011), "Design and experimental characterization of an electromagnetic transducer for large-scale vibratory energy harvesting applications", *J. Intel. Mat. Syst. Str.*, **22**(17), 2009-2024.
- Chuan, L., Liang, M., Wang, Y. and Dong, Y. (2012), "Vibration suppression using two terminal flywheel. Part I: Modeling and Characterization", *J. Vib. Control*, **18**(8), 1096-1105.
- De Angelis, M., Perno, S., Reggio, A. (2012), "Dynamic response and optimal design of structures with large mass ratio TMD", *Earthq. Eng. Struct. D.*, **41**(1), 41-60.
- Den Hartog, J.P. (1956), *Mechanical Vibrations*, McGraw-Hill (4th Ed.), New York, NY, USA.
- Dhand, A. and Pullen, K.R. (2015), "Analysis of continuously variable transmission for flywheel energy storage systems in vehicular application", *Proceedings of the Institution of Mechanical Engineers, Part C: Journal of Mechanical Engineering Science*, **229**(2), 273-290.
- Domizio, M., Ambrosini, D. and Curadelli, O. (2015), "Performance of TMDs on nonlinear structures subjected to near-fault earthquakes", *Smart Struct. Syst.*, **16**(4), 725-742.
- Frahm, H. (1911), *Device for Damping Vibrations of Bodies*, U.S. Patent 989958, USPTO.
- Krenk, S. (2005), "Frequency analysis of the tuned mass damper", *J. Appl. Mech. - ASME*, **72**, 936-942.
- Leung, A.Y.T. and Zhang, H. (2009), "Particle swarm optimization of tuned mass dampers", *Eng. Struct.*, **31**(3), 715-728.
- Lin, C.C., Wang, J.F. and Chen, B.L. (2005), "Train-induced vibration control of high-speed railway bridges equipped with multiple tuned mass dampers", *J. Bridge Eng. - ASCE*, **10**(4), 398-414.
- Ghosh, A. and Basu, B. (2007), "A closed-form optimal tuning criterion for TMD in damped structures", *Structural Control and Health Monitoring*, **14**(4), 681-692.
- Giaralis, A. and Petrini, F. (2017), "Wind-induced vibration mitigation in tall buildings using the tuned mass-damper-inerter (TMDI)", *J. Struct. Eng. - ASCE*, *accepted for publication*.
- Gonzalez-Buelga, A., Clare, L.R., Cammarano, A., Neild, S.A., Burrow, S.G. and Inman, D.J. (2014), "An optimised tuned mass damper/harvester device", *Structural Control and Health Monitoring*, **21**(8), 1154-1169.
- Gonzalez-Buelga, A., Lazar, I., Jiang, J.Z., Neild, S.A. and Inman, D.J. (2016), "Assessing the effect of nonlinearities on the performance of a Tuned Inerter Damper", *Struct. Control Health Monit.*, DOI: 10.1002/stc.1879.
- Hendijanizadeh, M., Shakh, S.M., Elliott, S.J. and Moshrefi-Torbati, M. (2013), "Output power and efficiency of electromagnetic energy harvesting systems with constrained range of motion", *Smart Mater. Struct.*, **22**(12), 125009.
- Hoang, N., Fujino, Y. and Warnitchai, P. (2008), "Optimal tuned mass damper for seismic applications and practical design formulas", *Eng. Struct.*, **30**, 707-715.
- Hu, Y. and Chen, M.Z.Q. (2015), "Performance evaluation for inerter-based dynamic vibration absorbers", *Int. J. Mech. Sci.*, **99**, 297-307.
- Hu, Y., Chen, M.Z.Q., Shu, Z. and Huang L. (2015), "Analysis and optimisation for inerter-based isolators via fixed-point theory and algebraic solution", *J. Sound Vib.*, **346**, 17-36, DOI:10.1016/j.jsv.2015.02.041.
- Hu, Y., Chen, M.Z.Q., Xu, S. and Liu Y. (2016), "Semiactive inerter and its application in adaptive tuned vibration absorbers", *IEEE T. Control Syst. Technol.*, DOI: 10.1109/TCST.2016.2552460.
- Jokic, M., Stegic, M. and Butkovic, M. (2011), "Reduced-order multiple tuned mass damper optimization: A bounded real lemma for descriptor systems approach", *J. Sound Vib.*, **330**, 5259-5268.
- Makihara, K., Hirai, H., Yamamoto, Y. and Fukunaga, H. (2015), "Self-reliant wireless health monitoring based on tuned-mass-damper mechanism", *Smart Struct. Syst.*, **15**(6), 1625-1642.
- Marian, L. and Giaralis, A. (2014), "Optimal design of a novel tuned mass-damper-inerter (TMDI) passive vibration control configuration for stochastically support-excited structural systems", *Probab. Eng. Mech.*, **38**, 156-164.
- Marian, L. and Giaralis, A. (2013), "Optimal design of inerter devices combined with TMDs for vibration control of buildings exposed to stochastic seismic excitations", *Proceedings of the 11th ICOSSAR International Conference on Structural Safety and Reliability for Integrating Structural Analysis, Risk and Reliability*, New York, June.
- Masri, S.F. and Caffrey, J.P. (2017), "Transient response of a SDOF system with an inerter to nonstationary stochastic excitation", *J. Appl. Mech. - ASCE*, **84**(4), 041005.
- Ormondroyd, J. and Den Hartog, J.P. (1928), "The theory of the dynamic vibration absorber", *J. Appl. Mech. - ASCE*, **50**, 9-22.
- Papageorgiou, C. and Smith, M.C. (2005), "Laboratory experimental testing of inerters", *Proceedings of the IEEE Conference on Decision and Control*, Seville, Spain, December.
- Pietrosanti, D., De Angelis M. and Basili, M. (2017), "Optimal design and performance evaluation of systems with Tuned Mass Damper Inerter (TMDI)", *Earthq. Eng. Struct. D.*, DOI:10.1002/eqe.2861.
- Rana, R. and Soong, T.T. (1998), "Parametric study and simplified design of tuned mass dampers", *Eng. Struct.*, **20**(3), 193-204.
- Ricciardelli, F. and Vickery, B.J. (1999), "Tuned vibration absorbers with dry friction damping", *Earthq. Eng. Struct. D.*, **28**(7), 707-724.
- Rome, L.C., Flynn, L., Goldman, E.M. and Yoo, T.D. (2005), "Generating electricity while walking with loads", *Science*, **309**(5741), 1725-1728.
- Salvi, J. and Rizzi, E. (2016), "Closed-form optimum tuning formulas for passive tuned mass dampers under benchmark excitations", *Smart Struct. Syst.*, **17**(2), 231-256.
- Shen, W., Zhu, S. and Xu, Y.I. (2012), "An experimental study on self-powered vibration control and monitoring system using electromagnetic TMD and wireless sensors", *Sensor. Actuat. - A*, **180**, 166-176.
- Shen, Z., Zhu, S., Zhu, H. and Xu, Y.L. (2016), "Electromagnetic energy harvesting from structural vibrations during earthquakes", *Smart Struct. Syst.*, **18**(3), 449-470.
- Smith, M.C. (2002), "Synthesis of mechanical networks: the inerter", *IEEE T. Autom. Control*, **47**(10), 1648-1662.
- Swift, S.J., Smith, M.C., Glover, A.R., Papageorgiou, C., Gartner, B. and Houghton, N.E. (2013), "Design and modelling of a fluid inerter", *Int. J. Control*, **86**(11), 2035-2051.
- Tang, X. and Zuo, L. (2012), "Simultaneous energy harvesting and vibration control of structures with tuned mass dampers", *J. Intel. Mat. Syst. Str.*, **23**(18), 2117-2127.
- Tributsch, A. and Adam, C. (2012), "Evaluation and analytical

- approximation of Tuned Mass Dampers performance in an earthquake environment”, *Smart Struct. Syst.*, **10**(2), 155-179.
- Wang, F.C., Hong, M.F. and Lin, T.C. (2011), “Designing and testing a hydraulic inerter”, *Proceedings of the Institution of Mechanical Engineers, Part C: Journal of Mechanical Engineering Science*, **225**(1), 66-72.
- Wang, J.F. and Lin, C.C. (2015), “Extracting parameters of TMD and primary structure from the combined system responses”, *Smart Struct. Syst.*, **16**(5), 937-960.
- Warburton, G.B. (1982), “Optimum absorber parameters for various combinations of response and excitation parameters”, *Earthq. Eng. Struct. D.*, **10**(3), 381-401.
- Xu, K. and Igusa, T. (1992), “Dynamic characteristics of multiple substructures with closely spaced frequencies”, *Earthq. Eng. Struct. D.*, **21**, 1059-1070.
- Yamaguchi, H. and Harnpornchai, N. (1993), “Fundamental characteristics of multiple tuned mass dampers for suppressing harmonically forced oscillations”, *Earthq. Eng. Struct. D.*, **22**(1), 51-62.
- Yang, F., Sedaghati, R. and Esmailzadeh, E. (2015), “Optimal design of distributed tuned mass dampers for passive vibration control of structures”, *Struct. Control Health Monit.*, **22**, 221-236.
- Zhu, S., Shen, W.A. and Zu, Y.L. (2012), “Linear electromagnetic devices for vibration damping and energy harvesting: Modeling and testing”, *Eng. Struct.*, **34**(1), 198-212.
- Zuo, L. (2009), “Effective and robust vibration control using series multiple tuned-mass dampers”, *J. Vib. Acoust.*, **131**(3), 031003.
- Zuo, L. and Tang, X. (2013), “Large-scale vibration energy harvesting”, *J. Intel. Mat. Syst. Str.*, **24**(11), 1405-1430.